

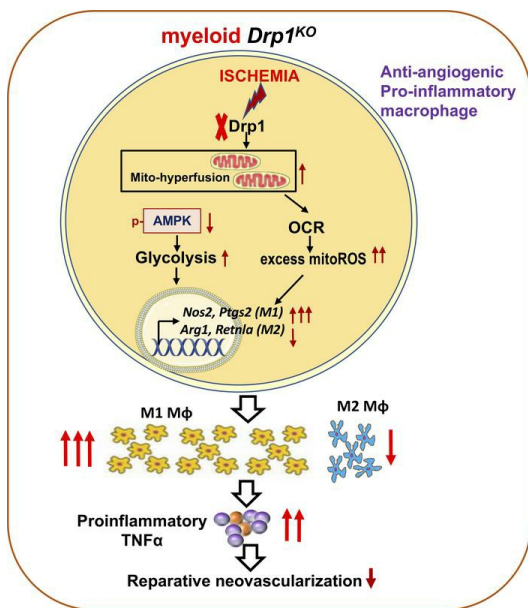
Myeloid Drp1 deficiency limits revascularization in ischemic muscles via inflammatory macrophage polarization and metabolic reprogramming

Shikha Yadav, ... , Tohru Fukai, Masuko Ushio-Fukai

JCI Insight. 2024. <https://doi.org/10.1172/jci.insight.177334>.

Research In-Press Preview Angiogenesis Inflammation

Graphical abstract



Find the latest version:

<https://jci.me/177334/pdf>



Myeloid DRP1 Deficiency Limits Revascularization in Ischemic Muscles via Inflammatory Macrophage Polarization and Metabolic Reprograming

Shikha Yadav¹, Vijay Ganta^{1,2}, Sudhahar Varadarajan^{1,3,4}, Vy Ong⁵, Yang Shi⁵, Archita Das^{1,3,4}, Dipankar Ash^{1,3}, Sheela Nagarkoti¹, Margorzata McMenamin^{1,4}, Stephanie Kelley¹, Tohru Fukai^{1,3,4}, Masuko Ushio-Fukai^{1,2}

¹Vascular Biology Center, ²Department of Medicine (Cardiology), ³Department of Pharmacology and Toxicology, Medical College of Georgia at Augusta University,

⁴Charlie Norwood Veterans Affairs Medical Center, Augusta GA 30912

⁵Biostatistics and Bioinformatics Core, Karmanos Cancer Institute, Department of Oncology, Wayne State University School of Medicine, Detroit, MI 48201.

Running Title: Macrophage DRP1 and angiogenesis

***Address correspondence to:**

Masuko Ushio-Fukai, Ph.D

Vascular Biology Center

Department of Medicine (Cardiology)

Medical College of Georgia at Augusta University

1460 Laney-Walker Blvd, CB-3212A

Augusta, GA 30912, USA

Email: mfukai@augusta.edu

ORCID iD <https://orcid.org/0000-0001-7048-2381>

Conflict of interest: The authors have declared that no conflict of interest exists.

Abstract

Macrophage plays a crucial role in promoting perfusion recovery and revascularization after ischemia through anti-inflammatory polarization, a process essential for the treatment of peripheral arterial disease (PAD). Mitochondrial dynamics, particularly regulated by the fission protein DRP1, are closely linked to macrophage metabolism and inflammation. However, the role of DRP1 in reparative neovascularization remains unexplored. Here we show that DRP1 expression was increased in F4/80⁺ macrophages within ischemic muscle at day 3 after hindlimb ischemia (HLI), an animal model of PAD. Mice lacking *Drp1* in myeloid cells exhibited impaired limb perfusion recovery, angiogenesis and muscle regeneration post-HLI. These effects were associated with increased pro-inflammatory M1-like macrophages, p-NFκB and TNFα, and reduced anti-inflammatory M2-like macrophages and p-AMPK in ischemic muscle of myeloid *Drp1*^{-/-} mice. *In vitro*, *Drp1*-deficient macrophages under hypoxia serum starvation (HSS), an *in vitro* PAD model, demonstrated enhanced glycolysis via reducing p-AMPK as well as mitochondrial dysfunction, and excessive mitochondrial ROS production, resulting in increased pro-inflammatory M1-gene and reduced anti-inflammatory M2-gene expression. Conditioned media from HSS-treated *Drp1*^{-/-} macrophages exhibited increased pro-inflammatory cytokine secretion, leading to suppressed angiogenesis in endothelial cells. Thus, macrophage DRP1 deficiency under ischemia drives pro-inflammatory metabolic reprogramming and macrophage polarization, limiting revascularization in experimental PAD.

Keywords: DRP1, mitochondrial fission, hindlimb ischemia, peripheral arterial disease, macrophage, inflammation, metabolic reprogramming

Introduction

Peripheral artery disease (PAD) poses a substantial burden of morbidity and mortality due to tissue damage resulting from acute and chronic occlusive ischemia (1, 2). Angiogenesis is the formation of new blood vessels from pre-existing ones, which requires endothelial cells (ECs) to proliferate, migrate, and differentiate to form new vascular structures and is indispensable for restoring limb perfusion of PAD (3). Therapeutic angiogenesis has faced multiple disappointments with clinical trials failing to demonstrate a difference in primary endpoint effects (4). Macrophage plays an important role in restoring perfusion recovery and revascularization following ischemia via anti-inflammatory polarization and producing angiogenic factors, which is required for treatment of PAD (5-9). In the early phases of the response to ischemic injury, a hypoxic and pro-inflammatory environment attracts pro-inflammatory M1-type macrophages characterized by enhanced aerobic glycolytic metabolism. Subsequently, a metabolic transition occurs, shifting macrophage phenotypes towards anti-inflammatory M2-type macrophages with increased oxidative phosphorylation in mitochondria, thus promoting reparative angiogenesis and neovascularization (10-13). Macrophage phenotype transition is a complex process influenced by tissue-specific and stimulus-specific differentiation, activation, and maturation programs (14). Defects in normal macrophage metabolism and polarization can lead to unresolved tissue injury, and exacerbation of tissue damage and impaired healing process (10, 11). The critical process of macrophage metabolic reprogramming for tissue repair is in part dependent on mitochondrial metabolism and dynamics (15); however, the underlying mechanisms in the context of ischemia-induced neovascularization are poorly understood.

Mitochondria are highly dynamic organelles that orchestrate metabolic and immune adaptations in response to ischemia. Prolonged ischemia can compromise cellular bioenergetics due to mitochondrial dysfunction (16). Mitochondrial dynamics, continuously adapting to extracellular stimuli, are tightly regulated by the mitochondrial fission proteins including dynamin-

related GTPase DRP1, Mitochondrial Fission Factor1 (MFF1) and mitochondrial fusion proteins including Mitofusins (MFN1 and MFN2) and optic atrophy1 (OPA1). Recent reports suggest the role of mitochondrial dynamics in regulating mitochondrial reactive oxygen species (mitoROS) levels, calcium homeostasis, and oxidative phosphorylation (17). Altered mitochondrial dynamics in macrophages are a universal response to a variety of inflammatory stimuli. In a context-dependent fashion, DRP1 plays a role in regulating pro- or anti-inflammatory macrophage phenotypes (18-22). It is shown that the inhibition of DRP1 using Mdivi-1 or *Drp1* siRNA transfection leads to a reduction in glycolysis, ROS production, and the NFkB-dependent pro-inflammatory M1-macrophage polarization when stimulated with lipopolysaccharide (LPS) (20). By contrast, DRP1 deficiency exacerbates LPS-induced systemic inflammation and liver injury in *in vivo* murine model (19). However, the role of macrophage DRP1 in reparative neovascularization during ischemia in an experimental PAD has not been reported.

In the present study using myeloid-specific *Drp1* knockout ($M\phi Drp1^{KO}$) mice with hindlimb ischemia (HLI) model, an animal model of PAD, we provide the evidence that $M\phi Drp1^{KO}$ mice exhibit impaired blood flow recovery, neovascularization, and muscle regeneration in response to HLI. This was associated with increased pro-inflammatory M1-like macrophage polarization, p-NFkB and TNF α and decreased anti-inflammatory M2-like macrophage polarization and phosphorylation of AMP-activated protein kinase (p-AMPK) in ischemic muscle. *In vitro* studies using bone marrow-derived macrophage (BMDM) from wild type (WT) and $M\phi Drp1^{KO}$ mice exposed to hypoxia serum starvation (HSS) showed that *Drp1*^{KO} BMDM under HSS had enhanced glycolysis via reducing p-AMPK. These cells also exhibited decreased mitochondrial oxygen consumption rate (OCR) and excessive mitoROS production, which in turn increased M1-genes and decreased M2-genes, and impaired angiogenic responses in cultured ECs. Our study will uncover macrophage DRP1 as a positive regulator and therapeutic target for promoting reparative neovascularization by enhancing anti-inflammatory macrophage polarization and metabolic reprogramming under ischemia.

Results

Myeloid DRP1 deficiency impairs reparative neovascularization via inhibiting angiogenesis and arteriogenesis in response to hindlimb ischemia (HLI). To assess the role of DRP1 in reparative neovascularization, we used the mouse HLI model which induces ischemia by femoral artery ligation and excision (23). Immunofluorescence analysis revealed that DRP1 was highly expressed in F4/80⁺ macrophages in ischemic muscles vs. non-ischemic muscles at day 3 after HLI (Figure 1A). To determine the role of macrophage DRP1 in post-ischemic neovascularization, we generated mice with myeloid-specific deletion of *Drp1* ($M\phi Drp1^{KO}$) by crossing homozygous *Drp1^{fl/fl}* mice with mice expressing Cre recombinase under control of the lysozyme M promoter (*LysM-Cre^{+/+}*) (Figure 1B). Selective deletion of DRP1 in macrophage was confirmed by protein analysis in bone marrow-derived macrophage (BMDM) and peritoneal macrophage, but not in the lungs or heart isolated from $M\phi Drp1^{KO}$ and WT mice (Figure 1C). Using laser speckle contrast perfusion imaging, we found no difference in blood flow recovery following HLI between *LysM-Cre^{+/+}/Drp1^{+/+}* WT and *LysM-Cre^{-/-}/Drp1^{fl/fl}* WT mice. In contrast, $M\phi Drp1^{KO}$ mice exhibited a reduction in blood flow recovery by day 21 post-HLI compared to both WT groups (Figure 1D). Immunohistochemical analysis revealed that $M\phi Drp1^{KO}$ mice had fewer CD31-positive capillary-like ECs (Figure 1E) and α -smooth muscle actin (α SMA)-positive arterioles (Figure 1F) in the ischemic gastrocnemius (GC) muscles compared to WT mice. However, there was no differences in CD31-positive ECs or α SMA-positive arterioles between the *LysM-Cre^{+/+}/Drp1^{+/+}* and *LysM-Cre^{-/-}/Drp1^{fl/fl}* WT groups (Figure S1A and S1B). H&E staining showed that increase in collateral lumen and wall area in semi-membranous muscle induced by HLI were reduced in $M\phi Drp1^{KO}$ mice (Figure 1G). This was associated with increased necrotic myofibers and delayed muscle regeneration in ischemic muscles of $M\phi Drp1^{KO}$ mice vs. WT mice (Figure 1H). Thus, macrophage DRP1 is required for restoring limb perfusion and promoting neovascularization by enhancing angiogenesis, arteriogenesis, tissue repair, and protection against necrosis in ischemic muscles following HLI.

Myeloid DRP1 deficiency increases pro-inflammatory M1-like macrophages and decreases anti-inflammatory M2-like macrophages without affecting the recruitment of Ly6C^{hi} monocytes in ischemic muscles. Macrophages are required for revascularization during HLI (5-9). To determine whether myeloid DRP1 regulates macrophage accumulation and polarization in ischemic hindlimbs, we performed immunofluorescence (IF) analysis. We observed an increase in F4/80⁺ macrophages in the ischemic muscles of WT mice on days 3 and 7 post-HLI, which was reduced in M ϕ Drp1^{KO} mice (Figure S2A). These findings were further confirmed by flow cytometry analysis, showing a reduction in CD45⁺/CD11b⁺/Ly6G⁻/Ly6C^{lo} monocytes-derived F4/80⁺/CD64⁺ macrophages isolated from the ischemic muscles of WT (*LysM-Cre/+* or *Drp1^{fl/fl}*) and M ϕ Drp1^{KO} mice on days 3 and 7 after HLI (Figure 2B).

We next examined the polarization of F4/80⁺ macrophages into CD80⁺ pro-inflammatory M1-like macrophages and CD206⁺ anti-inflammatory M2-like macrophages in ischemic muscles. The IF analysis demonstrated an increase in CD206⁺ M2-like macrophages and CD80⁺ M1-like macrophages in ischemic muscles of WT mice at days 3 and 7 post-HLI. However, in M ϕ Drp1^{KO} mice, the number of CD206⁺ M2-like macrophages was reduced at both time points (Figure S2B), while the number of CD80⁺ M1-like macrophages showed an increase on day 7 (Figure S2C) compared to WT mice. Co-localization analysis with F4/80⁺ cells revealed a decrease in F4/80⁺/CD206⁺ M2-like macrophages in M ϕ Drp1^{KO} mice on days 3 and day 7 post-HLI (Figure 2C). In contrast, F4/80⁺/CD80⁺ M1-like macrophages were elevated in M ϕ Drp1^{KO} mice on day 7 post-HLI compared to WT controls (Figure 2D). These findings were further confirmed by flow cytometry, which showed altered proportions of F4/80⁺/CD64⁺/CD206⁺ M2-like macrophages and F4/80⁺/CD64⁺/CD80⁺ M1-like macrophages in the ischemic muscles on days 3 and 7 post-HLI (Figure 2E), according to the gating strategy illustrated in Figure S3. Notably, Ly6C^{hi}-derived F4/80⁺/CD64⁺ mature macrophages were negligible, with no detectable M1- and M2-like macrophages at these points. These results suggest that F4/80⁺/CD64⁺ total macrophages originate from infiltrating CD45⁺/CD11b⁺/Ly6G⁻/Ly6C^{lo} monocytes.

We next examined whether myeloid DRP1 deficiency-induced decrease in F4/80⁺ macrophages in ischemic muscles was due to decrease in immune cells mobilization from bone marrow or their recruitment/infiltration or macrophages differentiation. To characterize the immune cells, we performed flow cytometry analysis in bone marrow (BM), peripheral blood and ischemic muscle after HLI (gating strategy and antibody panel are shown in Figure S3, Table 2). We found that the numbers of Ly6G⁺ neutrophils and Ly6C^{hi} monocytes in BM (Figure S4A) and peripheral blood (Figure S4B) were similar between WT and M ϕ Drp1^{KO} mice on days 3 and 7 after HLI. Figure S4C shows that, in ischemic muscles, the numbers of Ly6G⁺ neutrophils were increased in M ϕ Drp1^{KO} mice vs. WT mice while those of Ly6C^{hi} monocytes were similar between M ϕ Drp1^{KO} mice and WT mice at day 3 after HLI (Figure S4C). Then, both Ly6G⁺ neutrophils and Ly6C^{hi} monocytes were reduced by day 7. These findings suggest that loss of myeloid DRP1 limits the polarization of anti-inflammatory M2-like macrophages, which originate from CD45⁺/CD11b⁺/Ly6G⁻/Ly6C^{lo} monocytes, as well as the differentiation of Ly6C^{hi} monocytes into mature F4/80⁺/CD64⁺ macrophages. Importantly, this occurs without affecting the release of monocytes from the BM or their recruitment to the ischemic muscle. This in turn impairs ischemia-induced revascularization during HLI.

Myeloid DRP1 deficiency increases pro-inflammatory genes and signaling and decreases anti-inflammatory genes and signaling in ischemic muscle. To confirm further the role of myeloid DRP1 in regulating macrophage polarization during HLI, we isolated F4/80⁺ macrophages from ischemic muscle at day 3 after HLI and found that pro-inflammatory M1-marker genes including *Nos2*, *Ptgs2* and *Il-1b* were up-regulated. By contrast, anti-inflammatory M2-marker genes including *Arg1* and *Retnla* were downregulated in M ϕ Drp1^{KO} mice compared to WT mice (Figures 3A). This was associated with a decrease in pro-angiogenic growth factor genes such as *Vegf* and *Tgfb* in macrophages isolated from ischemic muscles of M ϕ Drp1^{KO} mice vs. WT mice (Figure 3A). Previous studies showed that pro-inflammatory NF κ B signaling and

anti-inflammatory AMPK signaling contribute to macrophage polarization toward M1- and M2-phenotype, respectively (24-27). We found that expression of p-NFκB, but not total NFκB protein, was increased in ischemic muscles on day 3 post-HLI of Mφ*Drp1*^{KO} mice vs. WT mice, which was associated with increased expression of pro-inflammatory TNFα (Figure 3B). In contrast, expression of p-AMPK, but not total AMPK protein, was reduced in ischemic tissues on day 3 post-HLI of Mφ*Drp1*^{KO} mice vs. WT mice (Figure 3C). Taken together, these results suggest that myeloid DRP1 deficiency enhanced the pro-inflammatory genes and p-NFκB-mediated M1-like macrophage axis, while decreased anti-inflammatory genes and p-AMPK signaling associated with M2-like macrophage polarization in ischemic muscles. This imbalance resulted in impaired reparative neovascularization following HLI.

***Drp1*^{KO} BMDM under HSS exhibit mitochondrial hyperfusion, which is associated with enhanced M1-macrophage polarization and reduced M2-macrophage polarization.** To explore the mechanisms by which DRP1 deficiency regulates macrophage polarization during ischemia, we performed *in vitro* studies using BMDMs isolated from WT and Mφ*Drp1*^{KO} mice, subjected to hypoxia serum starvation (HSS) as an *in vitro* model for PAD (Figure 4A), as previously described (28, 29). Mito-tracker staining revealed that WT-BMDMs under HSS induced mitochondrial fission, peaking at 1 to 2 hrs and returning to baseline levels by 8hrs (data not shown) (Figure S5A). However, HSS did not alter pSer616-DRP1, pSer637-DRP1, DRP1 protein levels, or the expression of the mitochondrial fission protein MFF1 or fusion proteins MFN1 and OPA1 in BMDMs (Figure S5B). In contrast, *Drp1*^{KO} BMDMs exhibited mitochondrial fusion at 2hr after HSS stimulation (Figure 4B). Electron microscopy further confirmed an increase in mitochondrial length and volume in Mφ*Drp1*^{KO} BMDMs following HSS stimulation compared to WT BMDMs (Figure S5C).

We next investigated the role of DRP1 in macrophage polarization using BMDM under *in vitro* HSS. Consistent with *in vivo* HLI model, HSS exposure to BMDMs increased M1 marker

gene *Nos2* and decreased M2 marker gene *Retnla* in a time-dependent manner (Figure S6A). *Drp1*^{KO} BMDMs with HSS exhibited enhanced M1-marker genes (*Nos2* and *Ptgs2*) and further decreased M2-maker genes (*Arg1* and *Retnla*) compared to *LysM-Cre* or *Drp1*^{fl/fl} (WT) BMDMs with HSS (Figure S6B). These findings suggest that loss of DRP1 in macrophage under HSS promotes pro-inflammatory macrophage polarization and reduces anti-inflammatory macrophage polarization *in vitro*. Given that we observed a reduction in the total number of F4/80⁺ macrophages in ischemic muscles of M ϕ *Drp1*^{KO} mice, we further investigated whether DRP1 deficiency affects macrophage proliferation or cell death under HSS *in vitro*. There was no difference in cell death, as determined by the CCK-8 assay, or in cell proliferation, assessed using the BrdU assay, between WT and *Drp1*^{KO} BMDMs under HSS (Figures S6C and S6D).

To further explore whether DRP1 promotes the expression of typical M2-like macrophage markers, we performed bulk RNA sequencing on BMDMs isolated from M ϕ *Drp1*^{KO} and *LysM-Cre*^{+/-}/*Drp1*^{+/+} (WT) mice following 8hrs of HSS stimulation (Figure S7). The volcano plot revealed 2,325 differentially expressed genes, with 1,208 up-regulated and 1,117 downregulated in *Drp1*^{KO} BMDMs compared to WT (Figure S7A). Notably, similar to the gene expression profile observed in macrophages isolated from ischemic muscle, WT BMDMs exhibited a coordinated upregulation of M2-associated and pro-angiogenic genes, while *Drp1*^{KO} BMDMs showed increased expression of M1-associated genes and decreased pro-angiogenic gene expression (Figure S7B). Gene Ontology (GO) (Figure S7C) and KEGG pathway (Figure S7D) enrichment analyses confirmed that pathways associated with an M2-like phenotype were more active in WT BMDMs. The identified GOs and KEGG pathways included genes involved in transcription, translation, cell activation, energy metabolism, intracellular transport, cell-cell interactions, and growth factors and cytokines linked to angiogenesis and muscle regeneration during ischemia (11, 30). These findings suggest that the loss of myeloid DRP1 impairs reparative M2 macrophage polarization under ischemic conditions.

***Drp1*^{KO} BMDMs under HSS exhibit hyperglycolysis through reduced AMPK activation, leading to increased M1-macrophage and decreased M2-macrophage polarization.** Since pro-inflammatory macrophage polarization is shown to undergo metabolic reprogramming from oxidative phosphorylation to aerobic glycolysis (12, 13), we measured the extracellular acidification rate (ECAR) using Seahorse assay. Figure 4C showed that *Drp1*^{KO} vs. WT BMDM under HSS exhibited increased glycolysis and glycolytic capacity. To address the mechanism by which DRP1 deficiency in macrophage under HSS enhances glycolysis, we measured p-AMPK which has been shown to promote anti-inflammatory and pro-angiogenic M2-macrophage polarization via suppression of glycolysis (26, 27). In line with observations in ischemic tissue *in vivo*, we found a reduction in p-AMPK and its substrates, detected by antibodies targeting the p-AMPK substrate motif (LXRXX(pS/pT)) in *Drp1*^{KO} BMDMs compared to WT BMDMs under HSS, but not under normoxia (Figures 4D, S8B and S8C). To determine whether decreased AMPK activity contributes to enhanced glycolysis and pro-inflammatory macrophage polarization in *Drp1*^{KO} BMDM under HSS, we performed rescue experiments using AMPK activator 5-aminoimidazole-4-carboxiamide ribonucleotide (AICAR) (27, 31). We found that activating AMPK by AICAR, at a concentration that did not affect glycolysis in WT BMDMs under HSS, restored the reduced p-AMPK and its substrates while enhancing glycolytic activity in *Drp1*^{KO} BMDMs under HSS (Figures 4E, S8B and S8C). Furthermore, this AMPK activation rescued the elevated expression of pro-inflammatory M1-genes *Nos2* and *Ptgs2* in *Drp1*^{KO} BMDM under HSS as comparable to those observed in HSS-exposed WT BMDM (Figure 4F). Notably, AICAR also rescued the reduced expression of genes associated with the anti-inflammatory M2 phenotype in *Drp1*^{KO} BMDM under HSS (Figure 4F). To address how DRP1 activates AMPK, we examined whether DRP1 regulates upstream AMPK kinases such as CAMKK and LKB1 in BMDMs exposed to HSS. We found a reduction in p-LKB1, but not that in p-CAMKK in HSS-stimulated *Drp1*^{KO} BMDMs compared to WT BMDMs (Figure S8A). These findings suggest that DRP1 activates AMPK through LKB1 in macrophages under ischemic conditions.

***Drp1*^{KO} BMDMs under HSS exhibit mitochondrial dysfunction and increased mitoROS production, leading to promoting M1-like macrophage polarization while inhibiting M2-like macrophage polarization.** Next, we examined the role of macrophage DRP1 in mitochondrial respiration by measuring OCR using the Seahorse assay. Figure 5A showed that *Drp1*^{KO} BMDMs under HSS exhibited a reduction in basal respiration, maximal respiration, and ATP production compared to WT BMDMs exposed to HSS. Note that basal OCR in both WT and *Drp1*^{KO} BMDMs under normoxic condition was not different (Figure S9A). This mitochondrial dysfunction was associated with excess mitoROS production in *Drp1*^{KO} BMDMs under HSS, as measured by MitoSOX fluorescence (Figure 5B). We then investigated the impact of increased mitoROS in *Drp1*^{KO} BMDMs on macrophage polarization under ischemic conditions. Our findings show that the mitochondria-specific O₂⁻ scavenger, Mito-TEMPO, reversed the elevated expression of pro-inflammatory M1-genes, *Nos2* and *Ptgs2*, and the reduced expression of the anti-inflammatory M2-gene *Retnla*, in *Drp1*^{KO} BMDMs under HSS. Mito-TEMPO had no effects on M1 or M2-gene expression in WT-BMDMs (Figure 5D) or on the elevated glycolysis (ECAR) in *Drp1*^{KO} BMDMs under HSS (Figure 5C). Notably, Mito-TEMPO restored the reduced basal respiration in *Drp1*^{KO} BMDMs, though it did not affect the decreased maximum respiration or ATP production of OCR, nor did it influence OCR in WT BMDMs (Figure S9B). These results suggest that elevated mitoROS in *Drp1*^{KO} macrophages under HSS contributes to reduced basal respiration and M2-like polarization while promoting M1-like polarization, without altering glycolysis. Additionally, activation of AMPK by AICAR did not mitigate the excess mitoROS production in *Drp1*^{KO} BMDM under HSS (Figure S9C). Consequently, our results suggest that the concurrent elevation of excess mitoROS and glycolysis coupled with reduced AMPK activation, collectively contribute to the promotion of M1-like macrophage polarization and the inhibition of M2-like macrophage polarization in *Drp1*^{KO} BMDM under HSS conditions.

Conditioned media from WT-BMDMs under HSS promotes angiogenesis in ECs, whereas media from *Drp1*^{KO} BMDMs under HSS does not. To investigate how myeloid DRP1 affects angiogenesis in ECs, we analyzed the impact of paracrine factors from the conditioned media of WT and *Drp1*^{KO} BMDMs exposed to HSS using *ex vivo* aortic ring and wound scratch assays (Figure 6A). Conditioned media from HSS-exposed WT-BMDMs, but not media from HSS-exposed *Drp1*^{KO} BMDMs, increased the number of sprouts in the aortic ring assay (Figure 6B). Additionally, conditioned media obtained from HSS-exposed WT-BMDMs, but not HSS-exposed *Drp1*^{KO} BMDMs, enhanced EC migration in a wound scratch assay with confluent EC cultures (Figure 6C). In contrast, conditioned media from normoxia-exposed WT or *Drp1*^{KO} BMDMs had a minimal effect on EC migration, with no difference between them (Figure 6C). The impaired pro-angiogenic effects of media from HSS-stimulated *Drp1*^{KO} BMDMs were associated with increased secretion of pro-inflammatory TNF α and IL-6 (Figure 6D). Notably, the impaired EC migration was restored when the conditioned media from HSS-stimulated *Drp1*^{KO} BMDMs was treated with an anti-TNF α antibody, but not with a control IgG (Figure 6E). These results suggest that elevated TNF α production by HSS-treated *Drp1*^{KO} macrophages contributes to reduced EC migration.

Discussion

Macrophages play a vital role in restoring perfusion and promoting revascularization after ischemia, largely due to their ability to polarize into anti-inflammatory M2 types and produce angiogenic factors. These functions are essential for the effective treatment of PAD (5-9). This study uncovers the myeloid DRP1 as a key regulator of reparative macrophage responses during ischemia, with potential for therapeutic neovascularization via anti-inflammatory macrophage polarization and metabolic reprogramming. Here we show that: 1) Myeloid-specific *Drp1*^{-/-} (M ϕ *Drp1*^{KO}) mice exhibited reduced limb perfusion, neovascularization and muscle regeneration in ischemic muscle after HLI. These effects are accompanied by increased pro-inflammatory M1-

like macrophage polarization, p-NF κ B, TNF α levels and decreased anti-inflammatory M2-like polarization and p-AMPK in the ischemic muscle microenvironment; 2) *In vitro*, *Drp1*^{KO} BMDMs exposed to HSS, an *in vitro* model of PAD, showed enhanced glycolytic activity due to reduced p-AMPK, along with mitochondrial dysfunction and excess mitoROS production, leading to increased M1 and decreased M2 gene expression; 3) Conditioned media from HSS-treated *Drp1*^{KO} BMDMs showed elevated pro-inflammatory cytokine secretion and suppressed angiogenic responses in cultured ECs.

Growing evidence highlights the critical role of mitochondrial dynamics as a key intracellular signaling platform for regulating innate immune responses (17, 32, 33). However, the specific role of macrophage DRP1 in inflammatory responses remains a subject of conflicting findings. Some studies suggest that lack of DRP1 in macrophages and microglia reduces inflammatory responses (18, 21). Furthermore, *in vivo* pharmacological inhibition of DRP1 with Mdivi-1, which is known to have off-target effects, including inhibition of Complex I activity (34), reduces cytokine production and mitigates inflammation in infections and inflammatory diseases (20, 35, 36). Notably, the impact of myeloid DRP1 varies across different pathological conditions. For instance, macrophage DRP1 promotes vascular injury-induced intimal thickening by enhancing pro-inflammatory responses (18), whereas liver-specific DRP1 deficiency accelerates LPS-induced acute liver injury by increasing inflammation (19). *In vitro* studies using DRP1 knockdown in macrophages have shown increased mitochondrial fusion and IL-1 β production via NLRP3 inflammasome activation (22). Therefore, the role of the mitochondrial fission protein DRP1 GTPase in modulating inflammatory phenotypes appears to depend on the context and cell type. Our current study provides the evidence to show the function of macrophage DRP1 in ischemia-induced neovascularization.

The present studies using myeloid *Drp1* deficient mice with HLI model, an experimental model of PAD, revealed that macrophage DRP1 plays a role in promoting reparative neovascularization in response to tissue ischemia. Flow cytometry and IF analysis found that

MφDrp1^{KO} mice showed reduction in CD45⁺/CD11b⁺/Ly6G⁻/Ly6C^{lo} alternative monocyte-derived naïve M0-like F4/80⁺/CD64⁺ macrophages and CD206⁺ M2-like macrophages at days 3 and 7 post-HLI, without affecting Ly6C^{hi} monocytes recruitment into ischemic muscles. Notably, *MφDrp1^{KO}* mice exhibited higher numbers of Ly6G⁺ neutrophils in the ischemic muscle at day 3 post HLI, followed by an increase in CD80⁺ M1-like macrophages and a decrease in M2-like macrophages by day 7. This aligns with previous studies of atherosclerotic plaques, where increased neutrophil promotes the differentiation of infiltrating monocytes into M1 macrophages (37, 38). Furthermore, it is shown that the enhanced clearance of infiltrated apoptotic neutrophils in ischemic muscles by macrophages contributes to the polarization of M2-macrophage, facilitating inflammation resolution and tissue regeneration (39). Notably, DRP1-mediated mitochondrial fission in macrophages is essential for the continuous clearance of apoptotic cells (40). Therefore, the elevated neutrophil in *MφDrp1^{KO}* ischemic muscles may further limit M2-macrophage polarization and neovascularization. These findings suggest that, in ischemic conditions, macrophage DRP1 is critical for promoting monocyte-to-macrophage differentiation, enhancing anti-inflammatory M2-like macrophage polarization, and suppressing pro-inflammatory macrophage polarization. In this study, we also used BMDMs isolated from WT and *MφDrp1^{KO}* mice with HSS stimulation, an *in vitro* model of PAD, and performed bulk RNA sequencing, along with volcano plot analysis, and GO and KEGG pathway assessments. The results suggest that pathways associated with an M2-like phenotype and pro-angiogenesis were upregulated in WT-BMDMs, while *Drp1^{-/-}* BMDMs exhibited increased expression of M1-related genes and decreased M2-related gene and pro-angiogenic gene expression.

Our study also found that macrophage DRP1 deficiency-driven impaired inflammatory M2-like macrophage phenotype in ischemic muscles is likely due to increasing the pro-inflammatory NFκB signaling and a concurrent decrease in the activation of the anti-inflammatory p-AMPK. This finding aligns with previous reports demonstrating the detrimental role of pro-inflammatory NFκB in hypoxia-induced ischemic brain injury and inflammation (24, 25). In

contrast, AMPK α 1 has been shown to promote HLI-induced arteriogenesis by regulating the production of angiogenic growth factors such as VEGF, TGF β , and FGF2 by M2-like macrophages (26, 27). Note that pro-inflammatory macrophages shift their metabolic profile from oxidative phosphorylation to aerobic glycolysis (12, 13). AMPK has been shown to promote anti-inflammatory and pro-angiogenic M2-macrophage polarization by suppressing pro-inflammatory glycolysis (26, 27). In line with our *in vivo* results in ischemic tissue, *in vitro* studies also demonstrated a reduction in AMPK activity, and enhanced induction of M1 genes *Nos2* and *Ptgs2* in *Drp1*^{KO} BMDMs under HSS when compared to WT-BMDMs. Consequently, conditioned media from M ϕ *Drp1*^{KO} macrophages exposed to HSS showed increased secretion of pro-inflammatory cytokines TNF α and IL-6, and exhibited impaired pro-angiogenic effects on cultured ECs compared to WT macrophages. Mechanistically, the reduced levels of p-AMPK and its substrate phosphorylation in *Drp1*^{KO} BMDM were linked to enhanced glycolysis, as demonstrated by the ECAR. This effect was reversed with the AMPK activator AICAR. Additionally, AMPK activation decreased the elevated expression of M1-genes *Nos2* and *Ptgs2* in *Drp1*^{KO} BMDM under ischemic conditions, while it increased the reduced expression of the M2-gene *Retnla*. We further investigated the mechanism by which DRP1 activates AMPK in macrophage under HSS. Our findings revealed that the upstream kinase of AMPK p-LKB1, but not p-CAMKK, was reduced in *Drp1*^{KO} BMDMs following HSS stimulation. These results suggest that DRP1 senses HSS signal by increasing p-LKB levels, thereby activating AMPK in macrophages.

It is unclear how DRP1 is activated in BMDMs in response to HSS without phosphorylation. DRP1 activity is known to be regulated by various post-translational modifications, such as phosphorylation, sumoylation, and S-nitrosylation at Cys644, among others (41, 42). This issue will be explored in more detail in future research. Additionally, the mechanism by which AMPK activation decreases glycolysis and pro-inflammatory macrophage polarization remains uncertain. It is reported that several downstream targets of AMPK suppress pro-

inflammatory signaling in macrophages. These include the activation of PI3 kinase or SIRT1, leading to the deacetylation and inhibition of NF κ B activity (26, 43). Additionally, the anti-inflammatory IL-10-mediated rapid activation of AMPK in macrophages is essential for the activation of the PI3K/Akt/mTORC1 and STAT3-mediated anti-inflammatory polarization of macrophages (26, 44). AMPK also is shown to downregulate inflammatory metabolism by inhibiting HIF1 α through the inactivation of mTORC1 (45). Further investigations are needed to elucidate the downstream targets of AMPK under ischemic conditions, which drive anti-inflammatory signaling in macrophages.

Mitochondrial functions are crucial for cellular metabolism under ischemic conditions, and prolonged ischemia exacerbates mitochondrial dysfunction (16). While the role of macrophage DRP1 in driving pro-inflammatory responses under bacterial LPS stimulation is well-documented (20, 36), its involvement in mitochondrial metabolism and inflammatory responses during ischemia remains unclear. For instance, after LPS stimulation, Drp1 activation in macrophages triggers excessive mitoROS production, which amplifies inflammatory cytokine release via NF κ B activation in a DRP1-dependent manner (20). In contrast, the present study demonstrates that *Drp1*^{KO} BMDMs exposed to HSS exhibited mitochondrial dysfunction, as evidenced by reduced OCR and increased mitoROS production. The mitoROS scavenger Mito-TEMPO restored the increased expression of M1-genes and decreased expression of M2-genes but did not impact the elevated glycolysis or reduced maximum respiration and ATP production of OCR in *Drp1*^{KO} BMDMs. These findings suggest that elevated mitoROS induced by *Drp1*^{KO} macrophages under HSS contributes to enhancing pro-inflammatory macrophage polarization and suppressing anti-inflammatory macrophage polarization without affecting glycolysis or OCR. It has been reported that AMPK and mitoROS can regulate each other (46, 47). For example, AMPK-mediated DRP1 regulation prevents EC dysfunction by suppressing mitoROS and ER stress (47). Under hypoxic conditions, mitoROS can directly activate AMPK through phosphorylation, independent of the AMP/ATP ratio (46). However, in current study, AICAR treatment did not reduce the elevated

mitoROS in *Drp1*^{KO} BMDMs under HSS. Thus, these findings suggest that in *Drp1*^{KO} BMDM exposed to HSS, hyperglycolysis is driven by the inhibition of AMPK activation independently of mitoROS, while excess mitoROS production occurs in parallel. These mechanisms may contribute to impaired neovascularization with enhanced M1- and reduced M2-macrophage polarization in M ϕ *Drp1*^{KO} mice (Figure 7).

To explore the role of myeloid DRP1 in angiogenesis of ECs, we examined the effects of paracrine factors from the conditioned media of WT and *Drp1*^{KO} BMDMs subjected to HSS on angiogenic responses. We utilized an *ex vivo* aortic ring assay and a wound scratch-induced EC migration assay for this purpose. Our results indicated that conditioned media obtained from HSS-treated *Drp1*^{KO} BMDM exhibited reduced pro-angiogenic function compared to that from HSS-treated WT-BMDMs, which was associated with increased secretion of pro-inflammatory cytokines, including TNF α and IL-6. Notably, the impaired migration of ECs was restored when the conditioned media from HSS-stimulated *Drp1*^{KO} BMDMs was treated with an anti-TNF α antibody. These findings indicate that pro-inflammatory cytokine, particularly TNF α released from HSS-stimulated *Drp1*^{KO} macrophages, contributes to impairing angiogenesis in ECs. This is in line with our *in vivo* observations and underscores the crucial role of macrophage DRP1 in facilitating communication between macrophages and ECs, which is necessary for reparative neovascularization following ischemia.

In summary, our findings underscore the essential role of macrophage DRP1-mediated mitochondrial dynamics in driving metabolic reprogramming towards anti-inflammatory macrophages, thereby enhancing neovascularization in response to ischemia. Specially, we have identified the activation of AMPK and the concurrent reduction in excessive mitoROS production as crucial downstream targets through which myeloid DRP1 orchestrates the metabolic reprogramming and mitochondrial functions of macrophages, fostering enhanced neovascularization and tissue repair in response to ischemic injury. Future studies will focus on exploring the role of endothelial DRP1 in ischemia-induced neovascularization (48). Furthermore,

[Type here]

177334-INS-RG-RV-3

given the encouraging outcomes from clinical trials using intramuscular cell therapy with BM mononuclear cells in patients with critical limb ischemia (4), our findings suggest that targeting macrophage DRP1 could be a promising therapeutic approach for treating PAD.

Methods

Sex as a biological variable. All experiments involving animals were conducted using both male and female mice at 8 to 12 weeks of age. No phenotype differences were observed between male and female mice in this study.

Animal Study. Room temperature and humidity were maintained at 22.5 °C and between 50% and 60%, respectively. All mice were held under the 12:12 (12-h light: 12-h dark) light/dark cycle. Mice were held in individually ventilated caging with a maximum of 5 or a minimum of 2 mice per cage. Myeloid-specific *Drp1*^{-/-} (MΦ*Drp1*^{KO}) mice were generated by crossing *Drp1*^{fl/fl} mice (provided by Dr. Hiromi Sesaki, Johns Hopkins University, Baltimore, Maryland, USA) with *LysM-Cre*^{Tg/Tg} mice (JAX, Stock No. 004781 on a C57BL/6J background). Male mice heterozygous for *Drp1* floxed allele and *LysM-Cre* transgene (*Drp1*^{fl/+} *LysM-Cre*^{Tg/+}) were crossed-bred with homozygous *Drp1* floxed female mice. The *LysM-Cre*^{+/-}/*Drp1*^{fl/fl} (MΦ*Drp1*^{KO}) genotype, as well as their littermate controls (*LysM-Cre*^{+/-}/*Drp1*^{+/+} or *LysM-Cre*^{-/-}/*Drp1*^{fl/fl}), were used for experiments.

Hindlimb ischemia model. Mice were subjected to unilateral hindlimb surgery under anesthesia with intraperitoneal administration of ketamine (87 mg/kg) and xylazine (13 mg/kg). We performed ligation and segmental resection of left femoral artery. Briefly, the left femoral artery was exposed, ligated both proximally and distally using 6-0 silk sutures and the vessels between the ligatures were excised without damaging the femoral nerve. Skin closure was done using 6-0 nylon sutures. We measured ischemic (left)/non-ischemic (right) limb blood flow ratio using a laser Doppler blood flow (LDBF) analyzer (PeriScan PIM 3 System; Perimed) as we reported (49, 50). Mice were anesthetized and placed on a heating plate at 37°C for 10 minutes to minimize temperature variation. Before and after surgery, LDBF analysis was performed in the plantar sole. Blood flow was displayed as changes in the laser frequency, represented by different color pixels, and mean LDBF values were expressed as the ratio of ischemic to non-ischemic LDBF.

Histological and Western blot analysis (Table 1 and 2). For cryosections, mice were euthanized and perfused through the left ventricle with saline, limbs were fixed in 4% paraformaldehyde (PFA) overnight and incubated with 30% sucrose, and gastrocnemius muscles were embedded in OCT compound (Sakura Finetek). 7 μ m cryosections for capillary density were stained with anti-mouse CD31 antibody (MEC 13.3, BD Bioscience). For immunohistochemistry, we used R.T.U. Vectorstain Elite (Vector Laboratories) followed by DAB visualization (Vector Laboratories). Arterioles were stained with Cy3-conjugated anti- α SMA antibody (1A4, Sigma). Macrophages were labeled with anti-F4/80 (BM8, Biolegend), M1-macrophage and M2-macrophages were labeled with anti-CD80 (16-10A1, Biolegend) and anti-CD206 (C068C2, Biolegend) antibody, respectively (Table 1). Images were captured by Keyence microscope (bz-x800) or confocal microscopy (Zeiss) and analyzed by Image J or LSM510 software (Zeiss), respectively. Western blot analysis was performed as previously described (23) (Table 2).

Isolation and primary culture of bone marrow derived macrophages (BMDMs). BM cells were harvested from hind leg tibiae and femur from 2x WT and *M ϕ Drp1^{KO}* mice and pooled. Briefly, BM cells were flushed from the bone with a 27G needle in DPBS and filtered using 70 μ m filter. Cells were cultured and differentiated in DMEM medium (Gibco) supplemented with antibiotics, 10% FBS and 20% conditioned media from L929 cell line (enriched in M-CSF) for 7 days in polystyrene culture plates and non-adherent cells were washed and removed every alternate day. The resulting BMDM population was determined by staining with anti-CD11b anti-Ly6C and anti-F4/80 antibodies and assessed by flow cytometry (Table 3).

In Vitro Hypoxia Serum Starvation (HSS). Cultured BMDMs were washed twice to remove traces of FCS and then incubated in starvation medium from Cell applications Inc. (Cat No: 209-250) and subjected to hypoxia (2% O₂) for indicated times (28, 29).

Conditioned medium preparation from HSS-stimulated BMDMs. Cultured BMDMs were exposed to HSS for 8 hr, and conditioned-medium (CM) was collected, filtered through 0.2 μ m filters, and

stored at -80°C with protease and peptidase inhibitor (Thermo Scientific, 1861280) until further use. Prior to the experiment, BMDM CM was thawed and concentrated using 3K Amicon ultra centrifugal tubes (UFC800396). Briefly, the CM was centrifuged at 4200 RPM for 8 min at 4°C . Total protein concentration was determined using the Bradford Assay.

Flow cytometry (FACS) analysis. (Table 3) Mouse whole blood and BM cells were collected by cardiac puncture and from femur and tibia respectively using 27G needle in EDTA coated 1mL syringe and placed in 1.5 mL EDTA coated Eppendorf tube for 30 min at room temperature (RT). The peripheral blood was spun down at 500 g for 1 min at 4°C . The supernatant was discarded, and the cells were re-suspended in 1 ml of RBC lysis buffer (00-4300-54, Invitrogen) for 10 min at RT in dark. Samples were then washed with DPBS with 2% FCS and centrifuged at 500 g for 5 min at 4°C . Cells were re-suspended in cold DPBS with 2% FCS and placed on ice. Excised gastrocnemius (GC) muscles were minced and enzymatically digested in DPBS containing collagenase type I 1 mg/mL Type I (C0130, Sigma), 18 mg/mL collagenase Type XI (C7657, Sigma), 1 mg/mL hyaluronidase (H3506, Sigma) and 50 U/mL DNase (D4263, Sigma) at 37°C for 1 hr. Cells were spun and re-suspended in DPBS with 2% FCS, followed by passing through 70 μm and 40 μm filter and counted. The cell suspension was incubated with blocking buffer consisting of anti-mouse CD16/CD32 (14-0161-85, eBioscience) and 2% FCS for 15 min in ice. Cells were stained with fluorophore-labeled specific antibodies for CD45, CD11b, Ly6G, Ly6C, F4/80, CD64, CD206, CD80, then incubated with a fixable viability dye for live cell gating (65-0866-14, Invitrogen) at 4°C for 30 min. Simultaneously, fluorophore-labeled isotype controls were used to exclude false positive-due to non-specific Ab binding. All antibodies were diluted at 1:100. Unstained cells and compensation beads (01-3333-42, Invitrogen) served as single-color controls for auto-compensation. After staining, cells were washed, fixed with 4% PFA, and analyzed using a ThermoFisher Attune Nxt flow cytometer (A24858 ThermoFisher Scientific). The recorded data was processed using FlowJO 10.10 software (BD Bioscience).

Isolation of macrophages from GC muscle. The GC muscles were minced and enzymatically digested as described. Cells were then magnetically labeled with an anti-F4/80 antibody and isolated through magnetic sorting (Miltenyi Biotec).

Wound scratch cell migration Assay. Confluent ECs, following 12 h of serum starvation (0.1% serum media), were scraped using sterilized 10- μ L pipette tips and then washed with 0.1% serum media (23). The ECs were incubated with CM (20ng/mL) derived from HSS-treated WT or Drp1^{-/-} BMDM 16 h with anti-TNF α antibody or IgG vehicle control. Images were captured immediately at 0 h and at 16 h after the wounding.

Ex vivo Aortic Ring Assay. Aortic rings from WT mice (1 mm in size) were prepared and placed in 48 well plate coated with growth factor-reduced Matrigel (Corning). The aortic rings were cultured for 5 days, with treatment every other day using CM (20ng/mL) derived from HSS-treated WT or Drp1^{-/-} BMDMs. Branch points or sprouting of aortic ring were quantified using ImagePro or Image J software (v 1 .52).

RNA Sequencing. BMDMs isolated from M ϕ Drp1^{KO} or *LysM-Cre^{+/+}/Drp1^{+/+}* (WT) mice simulated with HSS for 8 hr were used. Total RNA was extracted using the RNeasy kit (Qiagen, Germantown, MD, USA), and RNAs were quantified by spectrophotometry (ND-2000, NanoDrop, ThermoFisher, Waltham, MA, USA). The quality of RNAs was determined using electrophoresis (2100 Bioanalyzer, Agilent Technologies, Santa Clara, CA, USA) prior to next-generation sequencing in the Genome Technology Access Center (GTAC) at Washington University, St. Louis, MO, USA. Samples with RNA integrity number (RIN) values >8.0 were subjected to polyA selection, chemical fragmentation, random hexamer priming, cDNA synthesis, and adapter-ligation using the TruSeq RNA Library Prep Kit (Illumina, San Diego, CA, USA), followed by paired-end multiplexed sequencing (HiSeq 2500, Illumina) according to the manufacturer's instructions. 2.2.8.

RNA-Seq Analysis. The FASTQ RNA-Seq read files were quantified using Kallisto (v0.46.1, California Institute of Technology, Pasadena, CA, USA) with the transcriptome indices built on the cDNA FASTA files from Ensembl mouse genome assembly GRCm39. Genes with lower than 10 total read counts were filtered for subsequent differential expression analysis. Differential expression analysis was performed using R package DESeq2 (v1.32.0, The University of North Carolina at Chapel Hill, Chapel Hill, NC, USA) by comparing *Drp1*^{KO} and WT BMDM samples, and the differentially expressed genes were identified using fold change > 1.25 and p-value < 0.05. The Gene Ontology (GO) Consortium and Kyoto Encyclopedia of Genes and Genomes (KEGG) pathway databases were used to perform GO and pathway enrichment analysis using R package clusterProfiler (v4.0.2, Southern Medical University, Guangzhou, China).

Quantitative RT-PCR. Total RNA was prepared from cells or tissues using Tri Reagent (Molecular Research Center Inc.) and phenol/ chloroform. Reverse transcription was carried out using high-capacity cDNA reverse transcription kit (Applied biosystems) with 2 μ g of total RNA. The PCR was performed as per manufacturer's protocol using ABI Prism 7000 Sequence Detection System 26 (Applied Biosystems, CA) and the QuantiFast SYBR Green PCR kit (Qiagen) for specific genes. Primer sequences for q RT-PCR are listed in Table 4. The expression of genes was normalized and expressed as fold-changes relative to HPRT.

Statistical analysis. Each experiment was repeated at least 3 times and data are presented as mean \pm SEM. Comparison between two groups were analyzed by unpaired two tailed Student *t*-test. Experiments with more than 2 subgroups were analyzed by ANOVA followed by the Tukey post-hoc or Bonferroni multiple comparison analysis to specify the significance between group differences. Values of *p<0.05, **p<0.01, ***p<0.001 were considered statically significant. Statistical tests were performed using Graphpad Prism v10 (GraphPad Software, San Diego, CA).

Study approval. All animal studies were carried out following protocols approved by the institutional Animal Care Committee and institutional Biosafety Committee at Augusta University.

Data availability. Gene expression data are available under GEO accession numbers GSE280186. All raw data associated with findings presented in the manuscript are included in the Supporting Data Values file.

Author contributions

M.U.-F., T.F. and S.Y. designed the study; S.Y. (major), S.V., A.D., D.A., S.N., S.K., performed/assisted research; M.U.-F., T.F., S.Y., V.O., Y.S. analyzed data; Y.S., V.G., discussed data and provided inputs; M.M. and S.K. performed mouse genotyping; V.G. provided materials. M.U.-F., T.F. and S.Y. wrote the manuscript.

Acknowledgements

This work was supported by National Institute of Health (NIH) grants: P01HL160557 (to T.F., M.U.F), R01HL160014 (to M.U.-F.), R01HL1740414 (to T.F., M.U.-F., V.S.); R01HL147550, R01HL147550-S1, R01HL133613 (to M.U.-F., T.F.); American Heart Association (AHA) Transformational project Award 22TPA971863 (to T.F.), 24CDA (to A.D.); 22CDA (to D.A.); 22Postdoc (to S.N.); Veterans Administration (VA) Merit Review Award 2I01BX001232 (to T.F.). We would like to thank Dr. Hiromi Sesaki at John's Hopkins University for providing Drp1 floxed mice, the Georgia Cancer Center Flow Cytometry Core for maintaining and ensuring the smooth operation of the Attune analyzer, and the Electron Microscopy and Histology Core facilities at Augusta University for their assistance in data acquisition.

References

1. Farber A, and Eberhardt RT. The Current State of Critical Limb Ischemia: A Systematic Review. *JAMA Surg.* 2016;151(11):1070-7.
2. Gerhard-Herman MD, Gornik HL, Barrett C, Barshes NR, Corriere MA, Drachman DE, et al. 2016 AHA/ACC Guideline on the Management of Patients With Lower Extremity Peripheral Artery Disease: A Report of the American College of Cardiology/American Heart Association Task Force on Clinical Practice Guidelines. *Circulation.* 2017;135(12):e726-e79.
3. Annex BH, and Cooke JP. New Directions in Therapeutic Angiogenesis and Arteriogenesis in Peripheral Arterial Disease. *Circ Res.* 2021;128(12):1944-57.
4. Iyer SR, and Annex BH. Therapeutic Angiogenesis for Peripheral Artery Disease: Lessons Learned in Translational Science. *JACC Basic Transl Sci.* 2017;2(5):503-12.
5. Arras M, Ito WD, Scholz D, Winkler B, Schaper J, and Schaper W. Monocyte activation in angiogenesis and collateral growth in the rabbit hindlimb. *J Clin Invest.* 1998;101(1):40-50.
6. Takeda Y, Costa S, Delamarre E, Roncal C, Leite de Oliveira R, Squadrito ML, et al. Macrophage skewing by Phd2 haploinsufficiency prevents ischaemia by inducing arteriogenesis. *Nature.* 2011;479(7371):122-6.
7. Jetten N, Donners MM, Wagenaar A, Cleutjens JP, van Rooijen N, de Winther MP, et al. Local delivery of polarized macrophages improves reperfusion recovery in a mouse hind limb ischemia model. *PLoS One.* 2013;8(7):e68811.
8. Krishnasamy K, Limbourg A, Kapanadze T, Gamrekashvili J, Beger C, Hager C, et al. Blood vessel control of macrophage maturation promotes arteriogenesis in ischemia. *Nat Commun.* 2017;8(1):952.
9. Nahrendorf M, and Swirski FK. Abandoning M1/M2 for a Network Model of Macrophage Function. *Circ Res.* 2016;119(3):414-7.
10. Mouton AJ, DeLeon-Pennell KY, Rivera Gonzalez OJ, Flynn ER, Freeman TC, Saucerman JJ, et al. Mapping macrophage polarization over the myocardial infarction time continuum. *Basic Res Cardiol.* 2018;113(4):26.
11. Varga T, Mounier R, Horvath A, Cuvellier S, Dumont F, Poliska S, et al. Highly Dynamic Transcriptional Signature of Distinct Macrophage Subsets during Sterile Inflammation, Resolution, and Tissue Repair. *J Immunol.* 2016;196(11):4771-82.
12. Koo SJ, and Garg NJ. Metabolic programming of macrophage functions and pathogens control. *Redox Biol.* 2019;24:101198.
13. Soto-Herero G, Gomez de Las Heras MM, Gabande-Rodriguez E, Oller J, and Mittelbrunn M. Glycolysis - a key player in the inflammatory response. *FEBS J.* 2020;287(16):3350-69.
14. Okabe Y, and Medzhitov R. Tissue biology perspective on macrophages. *Nat Immunol.* 2016;17(1):9-17.

15. Wang Y, Li N, Zhang X, and Horng T. Mitochondrial metabolism regulates macrophage biology. *J Biol Chem.* 2021;297(1):100904.
16. Ueta CB, Gomes KS, Ribeiro MA, Mochly-Rosen D, and Ferreira JC. Disruption of mitochondrial quality control in peripheral artery disease: New therapeutic opportunities. *Pharmacol Res.* 2017;115:96-106.
17. Rambold AS, and Pearce EL. Mitochondrial Dynamics at the Interface of Immune Cell Metabolism and Function. *Trends Immunol.* 2018;39(1):6-18.
18. Umezu R, Koga JI, Matoba T, Katsuki S, Wang L, Hasuzawa N, et al. Macrophage (Drp1) Dynamin-Related Protein 1 Accelerates Intimal Thickening After Vascular Injury. *Arterioscler Thromb Vasc Biol.* 2020;40(7):e214-e26.
19. Wang L, Li X, Hanada Y, Hasuzawa N, Moriyama Y, Nomura M, et al. Dynamin-related protein 1 deficiency accelerates lipopolysaccharide-induced acute liver injury and inflammation in mice. *Commun Biol.* 2021;4(1):894.
20. Yu W, Wang X, Zhao J, Liu R, Liu J, Wang Z, et al. Stat2-Drp1 mediated mitochondrial mass increase is necessary for pro-inflammatory differentiation of macrophages. *Redox Biol.* 2020;37:101761.
21. Gao F, Reynolds MB, Passalacqua KD, Sexton JZ, Abuaita BH, and O'Riordan MXD. The Mitochondrial Fission Regulator DRP1 Controls Post-Transcriptional Regulation of TNF-alpha. *Front Cell Infect Microbiol.* 2020;10:593805.
22. Park S, Won JH, Hwang I, Hong S, Lee HK, and Yu JW. Defective mitochondrial fission augments NLRP3 inflammasome activation. *Sci Rep.* 2015;5:15489.
23. Das A, Ash D, Fouda AY, Sudhakar V, Kim YM, Hou Y, et al. Cysteine oxidation of copper transporter CTR1 drives VEGFR2 signalling and angiogenesis. *Nat Cell Biol.* 2022;24(1):35-50.
24. Wang N, Liang H, and Zen K. Molecular mechanisms that influence the macrophage m1-m2 polarization balance. *Front Immunol.* 2014;5:614.
25. Fong CH, Bebien M, Didierlaurent A, Nebauer R, Hussell T, Broide D, et al. An antiinflammatory role for IKKbeta through the inhibition of "classical" macrophage activation. *J Exp Med.* 2008;205(6):1269-76.
26. Sag D, Carling D, Stout RD, and Suttles J. Adenosine 5'-monophosphate-activated protein kinase promotes macrophage polarization to an anti-inflammatory functional phenotype. *J Immunol.* 2008;181(12):8633-41.
27. Mounier R, Théret M, Arnold L, Cuvellier S, Bultot L, Göransson O, et al. AMPK α 1 regulates macrophage skewing at the time of resolution of inflammation during skeletal muscle regeneration. *Cell Metab.* 2013;18(2):251-64.
28. Ganta VC, Choi M, Farber CR, and Annex BH. Antiangiogenic VEGF(165)b Regulates Macrophage Polarization via S100A8/S100A9 in Peripheral Artery Disease. *Circulation.* 2019;139(2):226-42.

29. Ganta VC, Choi M, Kutateladze A, and Annex BH. VEGF165b Modulates Endothelial VEGFR1-STAT3 Signaling Pathway and Angiogenesis in Human and Experimental Peripheral Arterial Disease. *Circ Res.* 2017;120(2):282-95.
30. Zhang J, Muri J, Fitzgerald G, Gorski T, Gianni-Barrera R, Masschelein E, et al. Endothelial Lactate Controls Muscle Regeneration from Ischemia by Inducing M2-like Macrophage Polarization. *Cell Metab.* 2020;31(6):1136-53 e7.
31. Giri S, Nath N, Smith B, Viollet B, Singh AK, and Singh I. 5-aminoimidazole-4-carboxamide-1-beta-4-ribofuranoside inhibits proinflammatory response in glial cells: a possible role of AMP-activated protein kinase. *J Neurosci.* 2004;24(2):479-87.
32. Benmoussa K, Garaude J, and Acin-Perez R. How Mitochondrial Metabolism Contributes to Macrophage Phenotype and Functions. *J Mol Biol.* 2018;430(21):3906-21.
33. Mehta MM, Weinberg SE, and Chandel NS. Mitochondrial control of immunity: beyond ATP. *Nat Rev Immunol.* 2017;17(10):608-20.
34. Bordt EA, Clerc P, Roelofs BA, Saladino AJ, Tretter L, Adam-Vizi V, et al. The Putative Drp1 Inhibitor mdivi-1 Is a Reversible Mitochondrial Complex I Inhibitor that Modulates Reactive Oxygen Species. *Dev Cell.* 2017;40(6):583-94 e6.
35. Li YH, Xu F, Thome R, Guo MF, Sun ML, Song GB, et al. Mdivi-1, a mitochondrial fission inhibitor, modulates T helper cells and suppresses the development of experimental autoimmune encephalomyelitis. *J Neuroinflammation.* 2019;16(1):149.
36. Nair S, Sobotka KS, Joshi P, Gressens P, Fleiss B, Thornton C, et al. Lipopolysaccharide-induced alteration of mitochondrial morphology induces a metabolic shift in microglia modulating the inflammatory response in vitro and in vivo. *Glia.* 2019;67(6):1047-61.
37. Prame Kumar K, Nicholls AJ, and Wong CHY. Partners in crime: neutrophils and monocytes/macrophages in inflammation and disease. *Cell Tissue Res.* 2018;371(3):551-65.
38. Soehnlein O, Zernecke A, Eriksson EE, Rothfuchs AG, Pham CT, Herwald H, et al. Neutrophil secretion products pave the way for inflammatory monocytes. *Blood.* 2008;112(4):1461-71.
39. Greenlee-Wacker MC. Clearance of apoptotic neutrophils and resolution of inflammation. *Immunol Rev.* 2016;273(1):357-70.
40. Wang Y, Subramanian M, Yurdagul A, Jr., Barbosa-Lorenzi VC, Cai B, de Juan-Sanz J, et al. Mitochondrial Fission Promotes the Continued Clearance of Apoptotic Cells by Macrophages. *Cell.* 2017;171(2):331-45 e22.
41. Chang CR, and Blackstone C. Dynamic regulation of mitochondrial fission through modification of the dynamin-related protein Drp1. *Ann N Y Acad Sci.* 2010;1201:34-9.
42. Otera H, Ishihara N, and Mihara K. New insights into the function and regulation of mitochondrial fission. *Biochim Biophys Acta.* 2013;1833(5):1256-68.
43. Yang Z, Kahn BB, Shi H, and Xue BZ. Macrophage alpha1 AMP-activated protein kinase (alpha1AMPK) antagonizes fatty acid-induced inflammation through SIRT1. *J Biol Chem.* 2010;285(25):19051-9.

44. Zhu YP, Brown JR, Sag D, Zhang L, and Suttles J. Adenosine 5'-monophosphate-activated protein kinase regulates IL-10-mediated anti-inflammatory signaling pathways in macrophages. *J Immunol*. 2015;194(2):584-94.
45. O'Neill LA, and Hardie DG. Metabolism of inflammation limited by AMPK and pseudo-starvation. *Nature*. 2013;493(7432):346-55.
46. Emerling BM, Weinberg F, Snyder C, Burgess Z, Mutlu GM, Viollet B, et al. Hypoxic activation of AMPK is dependent on mitochondrial ROS but independent of an increase in AMP/ATP ratio. *Free Radic Biol Med*. 2009;46(10):1386-91.
47. Li J, Wang Y, Wang Y, Wen X, Ma XN, Chen W, et al. Pharmacological activation of AMPK prevents Drp1-mediated mitochondrial fission and alleviates endoplasmic reticulum stress-associated endothelial dysfunction. *J Mol Cell Cardiol*. 2015;86:62-74.
48. Nagarkoti S, Kim YM, Das A, Ash D, E AV, Read TA, et al. Endothelial Drp1 Couples VEGF-induced Redox Signaling with Glycolysis Through Cysteine Oxidation to Drive Angiogenesis. *bioRxiv*. 2024.
49. Fang MM, Barman PK, Thirupathi M, Mirza RE, McKinney RD, Deng J, et al. Oxidant Signaling Mediated by Nox2 in Neutrophils Promotes Regenerative Myelopoiesis and Tissue Recovery following Ischemic Damage. *J Immunol*. 2018;201(8):2414-26.
50. Urao N, Razvi M, Oshikawa J, McKinney RD, Chavda R, Bahou WF, et al. IQGAP1 is involved in post-ischemic neovascularization by regulating angiogenesis and macrophage infiltration. *PLoS One*. 2010;5(10):e13440.

Figure legends

Figure 1: Myeloid *Drp1*^{KO} mice exhibited impaired reparative neovascularization via reducing angiogenesis and arteriogenesis in response to ischemia. **A.** Immunofluorescence analysis for Drp1 (red) or F4/80⁺ macrophage (green) expression and their co-localization in non-ischemic and ischemic gastrocnemius (GC) muscles at day 3 post-HLI. Scale bar=10 μ m. **B.** Schematic representation of breeding strategy for generating myeloid-specific Drp1^{-/-} (M ϕ Drp1^{KO}) mice by crossing *LysM-Cre* mice with *Drp1*^{fl/fl} mice. **C.** Immunoblotting (IB) for DRP1 protein expression in bone marrow-derived macrophage (BMDM), peritoneal macrophages (PM), lungs and heart isolated from Drp1^{fl/fl} (WT) and M ϕ Drp1^{KO} (M ϕ KO) mice. **D.** Upper panels show representative laser Doppler images of legs at day 0 and day 21. Lower panels show the blood flow recovery after HLI as determined by the ratio of foot perfusion between ischemic (left) and non-ischemic (right) legs in Drp1^{fl/fl}, *LysM-Cre* and M ϕ KO mice (n=8-12 mice per group, two-way ANOVA followed by Tukey's multiple comparison test). **E.** Immunohistochemical analysis for CD31⁺ staining (capillary density), n=4 mice per group, unpaired t test. **F.** Immunofluorescence analysis of α -smooth muscle actin⁺ staining (arterioles) in ischemic and non-ischemic GC muscles in WT and M ϕ KO mice at day 21 post-HLI. Scale bar=20 μ m, (n=5-6 mice per group, unpaired t test). The right panel shows quantification. **G.** H&E staining of ischemic and non-ischemic adductor (AD) muscles in WT and M ϕ KO mice at day 7 post-HLI. Arrow heads show collateral arteries. Scale bar=50 μ m, (unpaired t test). The right panels show quantification of diameter and wall thickness of collateral arteries. **H.** H&E staining of ischemic and non-ischemic GC muscles in WT and M ϕ KO mice at indicated times after HLI. The right panels show quantification of % of necrotic and regenerating myofiber in these muscles. Scale bar=20 μ m, (two-way ANOVA followed by Bonferroni's multiple comparison test). Data are mean \pm SEM. n=4-6. *p<0.05, **p<0.01, ***p<0.001.

Figure 2: Myeloid *Drp1*^{KO} mice exhibited increase in pro-inflammatory M1-like macrophages and decrease in anti-inflammatory M2-like macrophages in ischemic muscles. **A.** Scheme

showing FACS based F4/80⁺ macrophage characterization from ischemic GC muscle in WT and *MφKO* mice following HLI. **B.** Representative flow cytometry contour plots and quantification of numbers of F4/80⁺/CD64⁺ macrophages isolated from ischemic GC muscles in WT and *MφKO* mice at indicated times post-HLI. **C and D.** Immunofluorescence analysis of F4/80⁺ (green) CD206⁺ (red) M2-like macrophages (**C**) or F4/80⁺ (green) CD80⁺ (pink) M1-like macrophages (**D**) with DAPI (blue) in ischemic GC muscles in WT and *MφKO* mice at indicated times post-HLI. Scale bar=20μm, bottom panels show quantification (two-way ANOVA followed by Bonferroni's multiple comparison test). **E.** Representative flow cytometry contour plots, histograms and (**F**) quantification of CD45⁺/CD11b⁺/F4/80⁺CD64⁺/CD206⁺ M2-like macrophage and CD45⁺/CD11b⁺ F4/80⁺/CD64⁺/CD80⁺ M1-like macrophage numbers in ischemic GC muscles in WT and *MφKO* mice at indicated time post-HLI, (two-way ANOVA followed by Bonferroni's multiple comparison test). Data are mean ± SEM. n=4-6. *p<0.05, **p<0.01, ***p<0.001. Note CD80⁺CD206⁺ double positive Mφ in M1/M2 contour plots (E) are not considered in quantification shown in F.

Figure 3: Myeloid *Drp1*^{KO} mice exhibited increase in pro-inflammatory genes and signaling and decrease in anti-inflammatory genes and signaling in ischemic muscle. **A.** Left, schematic representation of magnetic bead based F4/80⁺ macrophage purification from ischemic GC muscle at day 3 post-HLI. These macrophages were used to analyze the pro-inflammatory genes (*Nos2*, *Ptgs2* and *Il1b*), anti-inflammatory genes (*Arg1* and *Retnla*) and pro-angiogenic growth factor genes (*Vegf* and *Tgfb*) mRNAs using quantitative qRT-PCR (fold increase relative to *Hprt*) in WT and *MφKO* mice at day 3 post-HLI (n=4-5 mice per group, unpaired t test). **B and C.** Western blot analysis of pro-inflammatory markers (p-NFκB, NFκB), (TNFα, actin (the loading control)) (n=3-6 mice per group) (B), and anti-inflammatory markers (p-AMPK and AMPK) (n=6 mice per group) (C), in ischemic tibialis anterior (TA) muscles of WT and *MφKO* mice on day 3 post-HLI. Blots for panels B and C were run separately on different gels using the same biological samples

(unpaired t test). The right panels show the quantification. Data are mean \pm SEM. * p <0.05, ** p <0.01, *** p <0.001.

Figure 4: *Drp1*^{KO} BMDM under HSS exhibited mitochondrial hyperfusion and hyperglycolysis, which was associated with decreased M2-like macrophages via reducing p-AMPK. **A.** Schematic representation showing cultured mouse BMDM exposed to hypoxia serum starvation (HSS), an *in vitro* PAD model. BMDM from WT and M ϕ KO mice were cultured for 7 days and then exposed to HSS. **B.** Analysis of mitochondrial structure by Mito-tracker green staining in WT and M ϕ KO BMDM with or without HSS stimulation for 2 h. Right panel shows quantification of mitochondrial length (n=number of cells analyzed from 3 independent exp.) by Image J. Scale bar=5 μ m, (one-way ANOVA followed by Tukey's multiple comparison test). **C.** Analysis of glycolysis measured by extracellular acidification rate (ECAR) using Seahorse XF analyzer in WT and M ϕ KO BMDM under HSS for 2 h. Right panels show quantification n=3, (unpaired t test). **D.** Western blot analysis for p-AMPK and AMPK expression in WT and M ϕ KO BMDM with HSS stimulation for 2 h and 8 h. Right panels show quantification. n=4-5, (unpaired t test). **E and F.** Effects of AMPK activator AICAR (pre-treatment for 2 h at 100 μ M) on glycolysis (ECAR) measured by Seahorse XF analyzer (E) (n=3, one-way ANOVA followed by Tukey's multiple comparison test). As well as mRNA expression for M1-markers (*Nos2* and *Ptgs2*) and M2-marker *Retnla* measured by qRT-PCR (F) (n=4, one-way ANOVA followed by Tukey's multiple comparison test) in WT and M ϕ KO BMDM under HSS for 2 h (E) or 8 h (F). Data are mean \pm SEM. * p <0.05, ** p <0.01, *** p <0.001.

Figure 5: *Drp1*^{KO} BMDM under HSS induced mitochondrial dysfunction and mitochondrial ROS (mitoROS) production, which in turn promoted M1-like macrophage polarization and reduced M2-like macrophage polarization. **A.** Analysis of mitochondrial respiration measured by OCR using Seahorse XF analyzer in WT and M ϕ KO BMDM under HSS for 2 h. Right panels show quantification (n=3, unpaired t test). **B.** Mitochondrial ROS production measured by

MitoSOX under normoxia or HSS for 2 h and 8 h in WT and M ϕ KO BMDM. Right panels show the averaged fluorescence intensity quantified by Image J. Scale bars=5 μ m, (n=number of cells analyzed from 3 independent exp., two-way ANOVA followed by Tukey's multiple comparison test). **C and D.** Effects of mito-TEMPO (pre-treatment of 16 h at 20 μ M) on glycolysis (ECAR) using Seahorse assay, n=3 (C) as well as mRNA expression for M1-markers (*Nos2* and *Ptgs2*) and M2-marker *Retnla* measured by qRT-PCR (D) (n=3-4, one-way ANOVA followed by Tukey's multiple comparison test) in WT and M ϕ KO BMDM under HSS for 2 h (C) or 8 h (D). Data are mean \pm SEM. *p<0.05, **p<0.01, ***p<0.001.

Figure 6: Conditioned medium (CM) from HSS-stimulated WT-BMDMs, but not from *Drp1*^{KO} BMDMs, promoted angiogenesis in ECs. **A.** Schematic representation of the isolation of CM from HSS-stimulated mouse BMDMs and its application on aortic ring assay and confluent HUVECs subjected to a wound scratch assay. **B.** Aortic ring assay showing the number of sprouts emerging from 1 mm aortic rings derived from WT mice, embedded on Matrigel, and incubated with CM (20ng/ml) from HSS-stimulated WT or M ϕ KO BMDMs for 5 days. Scale bars=1mm, (n=4, one-way ANOVA followed by Tukey's multiple comparison test). **C.** EC migration using the wound-scratch assay on confluent HUVEC monolayers treated with CM from WT or M ϕ KO BMDMs exposed to normoxia or HSS for 8 h. Representative bright field images (left) and quantification of number of migrated cells per field (right) in HUVECs at 16 h after wound scratch. Scale bars=20 μ m. (n=4, one-way ANOVA followed by Tukey's multiple comparison test). **D.** Representative protein expression of pro-inflammatory markers TNF α and IL-6 and respective Ponceau staining in CM from WT or M ϕ KO BMDMs stimulated with HSS for 8 h. Blots were run separately on different gels using the same biological samples. Right panels show quantification. (n=4, unpaired t test). **E.** EC migration using the wound-scratch assay on confluent HUVEC monolayers treated with CM from WT or M ϕ KO BMDMs stimulated with HSS for 8 h in the presence of either IgG (control) or anti-TNF α antibody (1 μ g/mL). Representative bright field images (left) and quantification of number of migrated cells per field (right) for HUVECs at 0 h

and 16 h after wound scratch. Scale bars=20 μm . (n=4, one-way ANOVA followed by Bonferroni's multiple comparison test). Data are mean \pm SEM. *p<0.05, **p<0.01, ***p<0.001.

Figure 7. Schematic model illustrating that DRP1 deficiency in macrophages under ischemia induces metabolic reprogramming characterized by hyperglycolysis. This occurs due to reduced AMPK activation and a mitochondrial dysfunction-excess mitoROS axis, leading to an increase in pro-inflammatory M1-like macrophage polarization and a decrease in anti-inflammatory M2-like macrophage polarization. Consequently, this impairs reparative neovascularization in response to ischemic injury.

Table 1: Antibodies used for histological and immunofluorescent analysis

Antigen	Conjugate	Species	Clone	Company	Catalog No.
CD31	Purified	Rat	MEC13.3	BD Pharmingen	550274
Actin, α -Smooth Muscle	Cy3	Mouse	1A4	Sigma	C6198
CD206	PE	Rat	C068C2	Biolegend	141705
CD80	AF647	Armenian Hamster	16-10A1	Biolegend	104718
F4/80	FITC	Rat	BM8	Biolegend	123107
Rat IgG	Biotin	Rabbit	Polyclonal	Vector laboratories	BA-4001
Rat IgG	AF488	Goat	Polyclonal	Invitrogen	A11006

Table 2: Antibodies used for western blot analysis

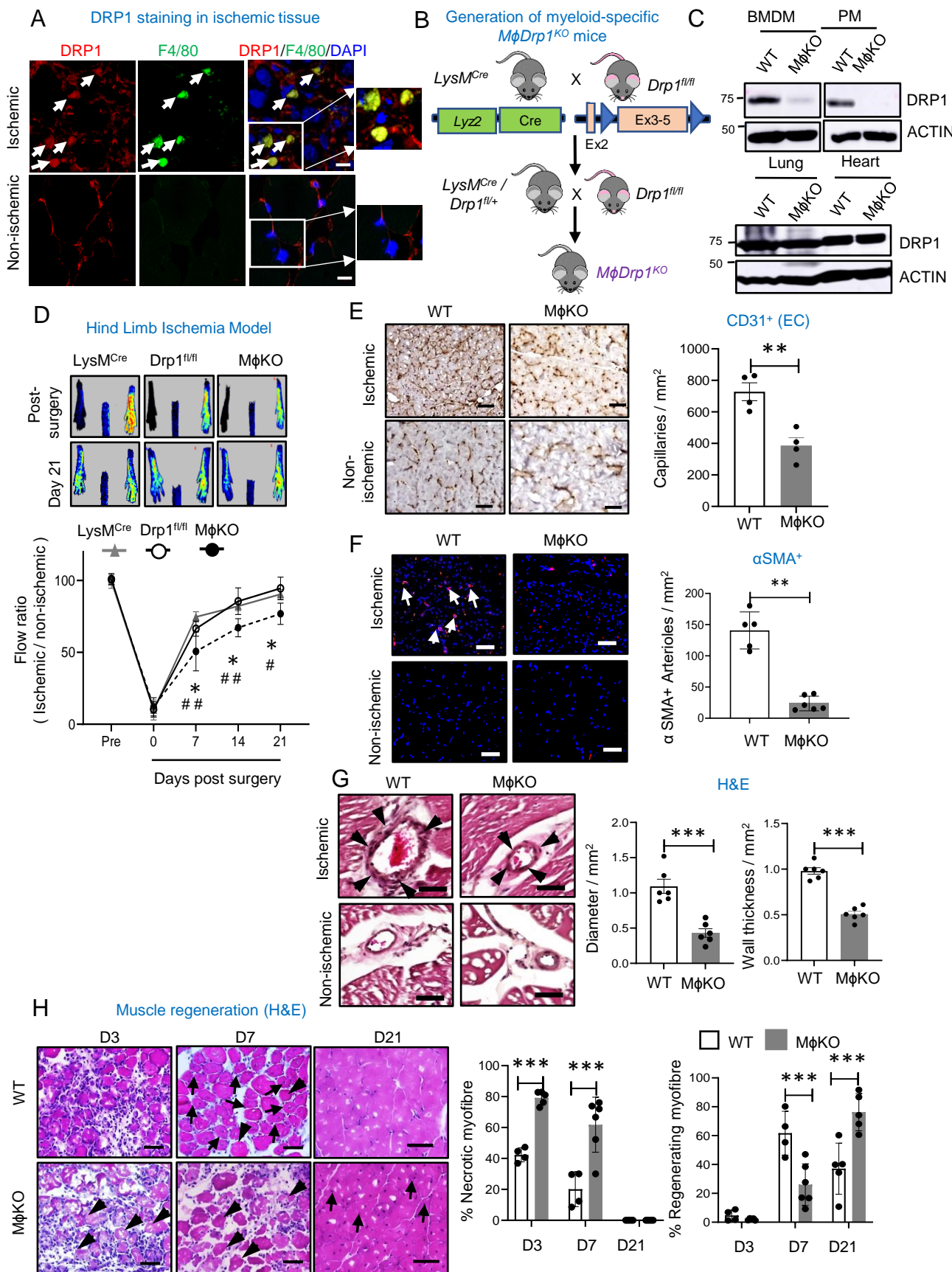
Antigen	Conjugate	Species	Clone	Company	Catalog No.
Phospho-DRP1 (Ser637)	Purified	Rabbit	Polyclonal	Cell Signaling	4867
Phospho-DRP1 (Ser616)	Purified	Rabbit	D9A1	Cell Signaling	4494
Phospho-AMPK α (Thr172)	Purified	Rabbit	40H9	Cell Signaling	2535
AMPK α	Purified	Rabbit	Polyclonal	Cell Signaling	2532
Phospho-NF- κ B p65 (Ser536)	Purified	Rabbit	93H1	Cell Signaling	3033
NF- κ B p65	Purified	Rabbit	D14E12	Cell Signaling	8242
Phospho-AMPK Substrate Motif	Purified	Rabbit	LXRX(pS/pT)	Cell Signaling	5759
Phospho-CaMKK2 Ser495	Purified	Rabbit	Polyclonal	Cell Signaling	16737
CaMKK2	Purified	Rabbit	D8D4D	Cell Signaling	16810
Phospho-LKB1 (Ser428)	Purified	Rabbit	C67A3	Cell Signaling	3482
LKB1	Purified	Mouse	Ley 37D/G6	Santa Cruz	SC- 32245
DRP1	Purified	Mouse	C-5	Santa Cruz	SC-271583
ACTIN	Purified	Mouse	C4	Santa Cruz	SC-47778
TNF α	Purified	Rabbit	Polyclonal	Abcam	ab66579
IL6	Purified	Goat	Polyclonal	R&D systems	AF-406-NA

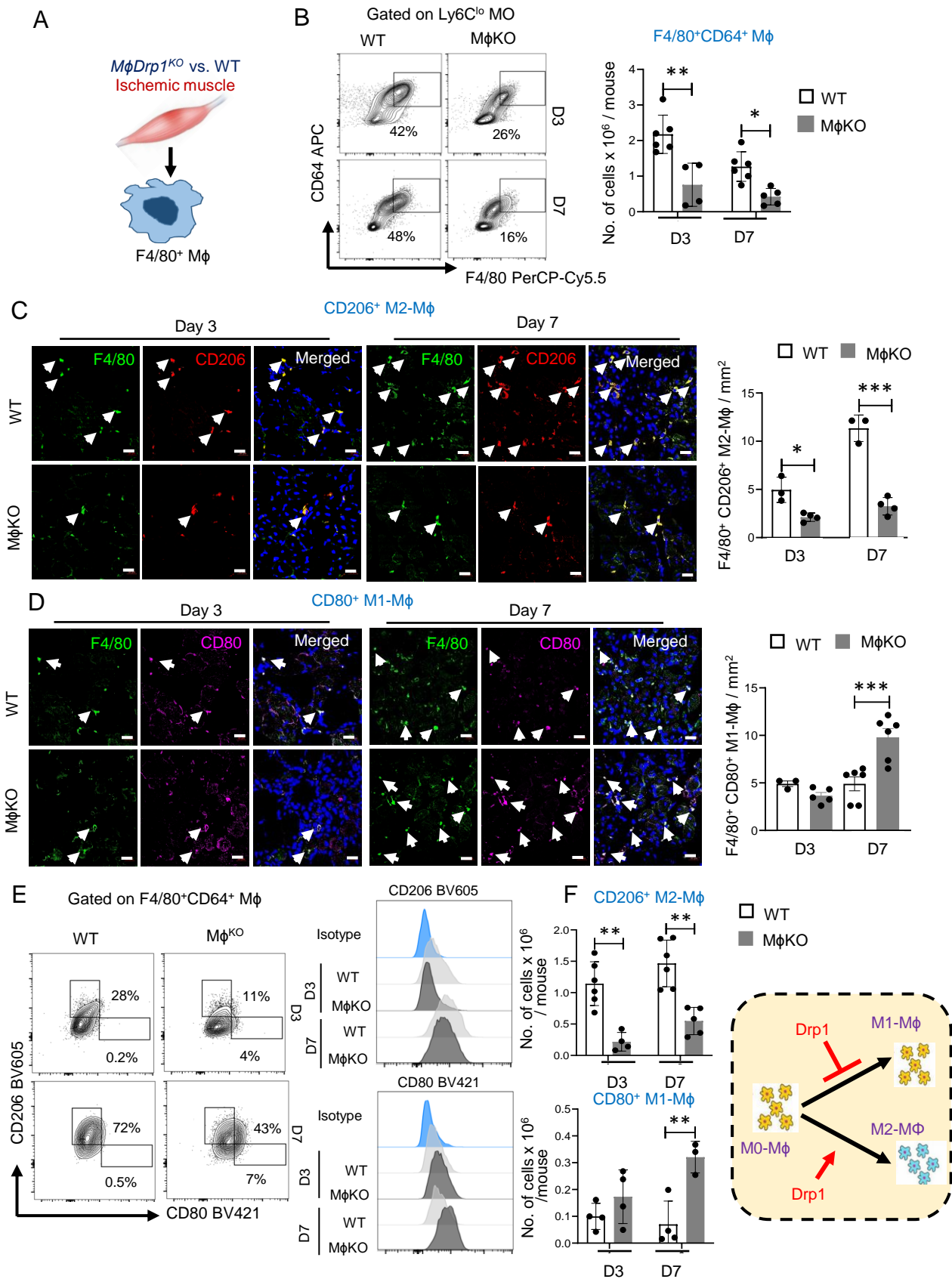
Table 3: Antibodies used for flow cytometry analysis

Antigen	Conjugate	Species	Clone	Company	Catalog No.
CD45	PE	Rat	<u>I3/2.3</u>	Biolegend	147712
CD11b	PE/Cyanine	Rat	<u>M1/70</u>	Biolegend	101216
CD11b	PE	Rat	M1/70	Invitrogen	12-0112-82
Ly6C	FITC	Rat	AL-21	BD Bioscience	553104
Ly6G	Alexa 647	Rat	1A8	Biolegend	127610
Ly6G	APC-Cyanine7	Rat	1A8	Biolegend	127624
F4/80	PerCP- Cyanine5.5	Rat	BM8	Invitrogen	45-4801-80
F4/80	APC	Rat	BM8	Biolegend	123116
CD80	BV421	Armenian Hamster	16-10A1	BD Bioscience	562611
CD206	BV650	Rat	C068C2	Biolegend	141721
CD64	APC	Mouse	X54-5/7.1	Biolegend	139306
IgG2a kappa Isotype control	PerCP- Cyanine5.5	Rat	Ebr2a	Invitrogen	45-4321-80
IgG1, ^k Isotype Ctrl	APC	Mouse	MOPC-21	Biolegend	400119
IgG2a, ^k Isotype Ctrl	BV605	Rat	RTK2758	Biolegend	400539
IgG2, ^k Isotype Control	BV421	Armenian Hamster	B81-3	BD Bioscience	562612

Table 4: Sequence of primers used for q-RT-PCR analysis.

Gene	Forward Primer	Reverse Primer
<i>Nos2</i>	TGAAGAAAACCCCTTGTGCT	TTCTGTGCTGTCCCAGTGAG
<i>Ptgs2</i>	ACTGGGCCATGGAGTGGACTTAAA	AACTGCAGGTTCTCAGGGATGTGA
<i>Arg1</i>	CATTGGCTTGCAGACGTAGAC	GCTGAAGGTCTCTCCATCACC
<i>Retnla</i>	CCCTGCTGGGATGACTGCTA	TGCAAGTATCTCCACTCTGGATCT
<i>Il1b</i>	GATGAAGGGCTGCTTCCAAAC	GTGCTGCTGCGAGATTTGAA
<i>Tgfb</i>	AACAACGCCATCTATGAGAAAACC	CCGAATGTCTGACGTATTGAAGAA
<i>Vegf</i>	AAAGGCTTCAGTGTGGTCTGAGAG	GGTTGGAACCGGCATCTTTATC
<i>Hprt</i>	CTGGTGAAAAGGACCTCTCGAAG	CCAGTTTCACTAATGACACAAACG

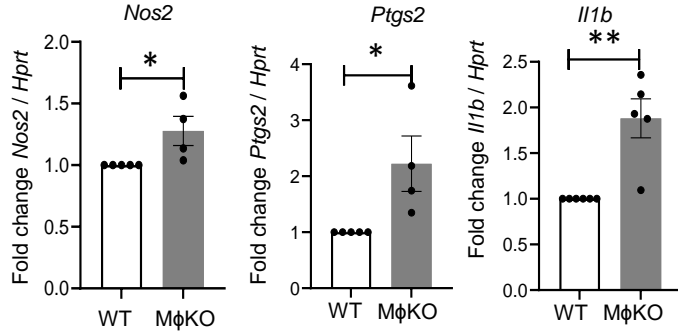
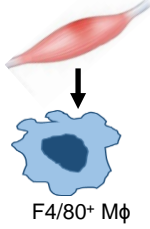




A

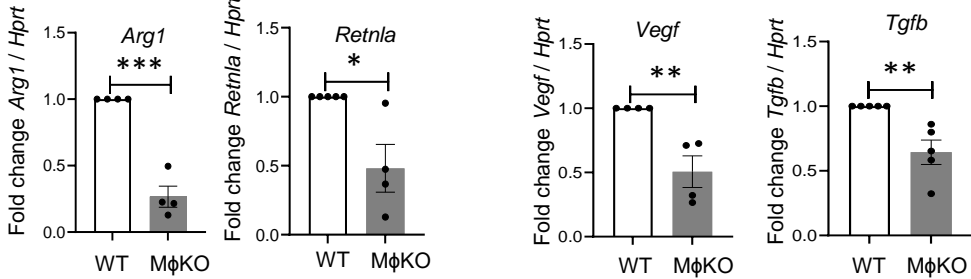
M1-marker genes in M ϕ from ischemic muscle

M ϕ Drp1^{KO} vs. WT
Ischemic muscle



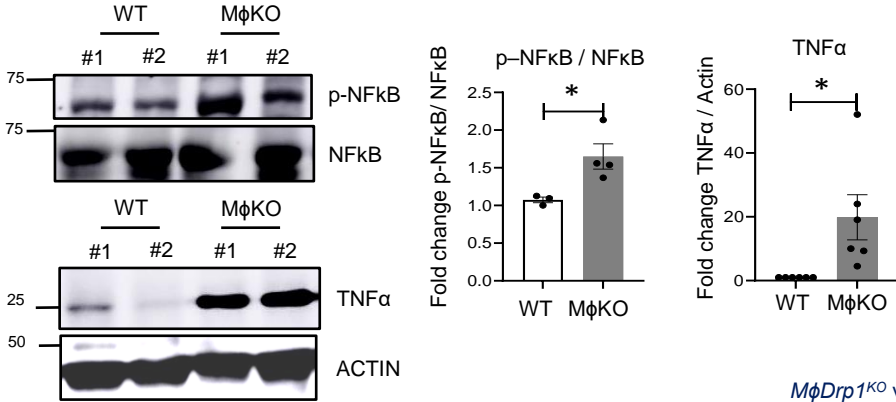
M2-marker gene

Growth factor gene



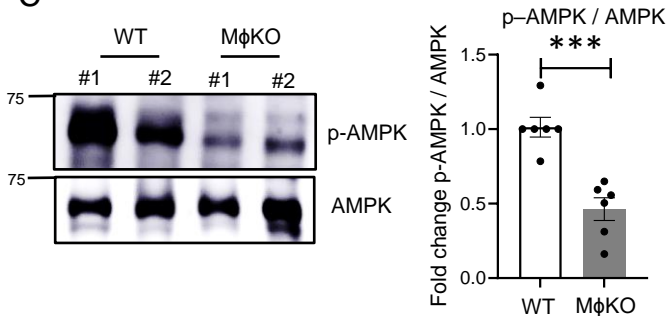
B

Ischemic muscle

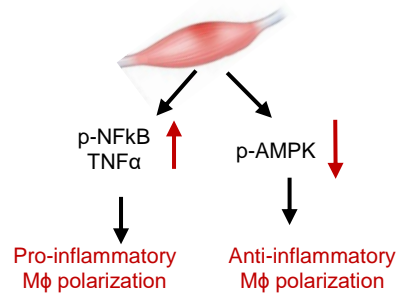


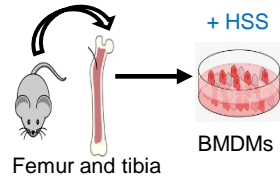
C

Ischemic muscle

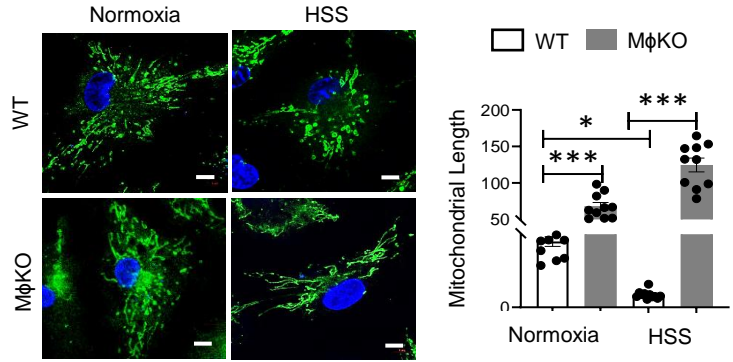


M ϕ Drp1^{KO} vs. WT
Ischemic muscle

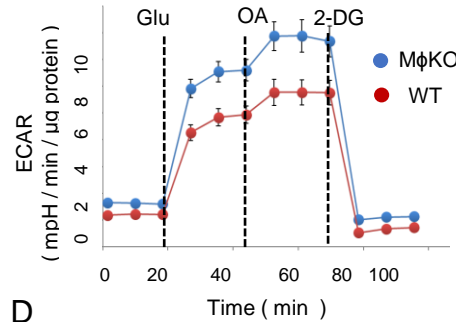


A**B**

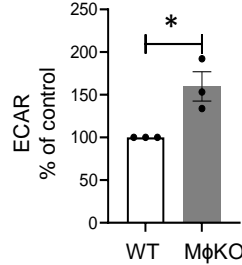
Mitochondrial structure (Mito-Tracker)

**C**

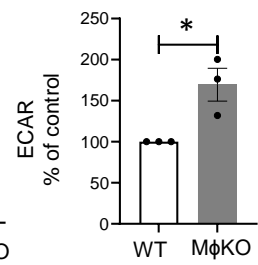
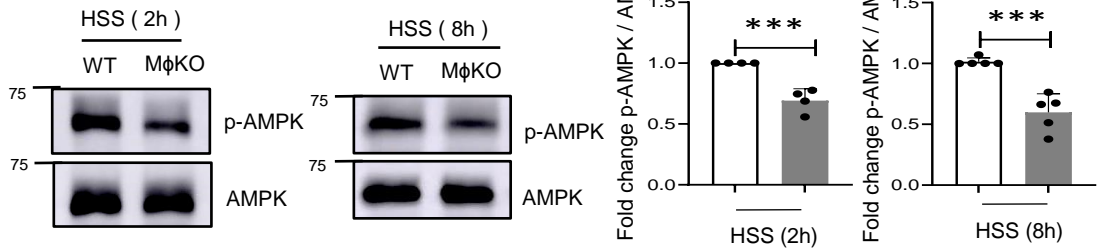
Glycolysis (ECAR)



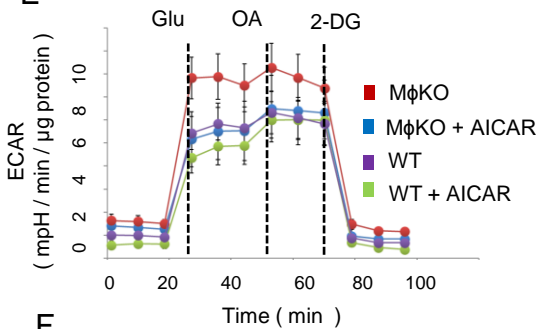
Glycolysis



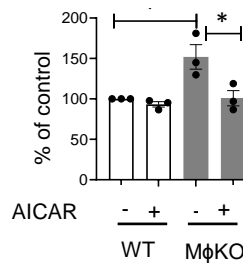
Glycolytic capacity

**D****E**

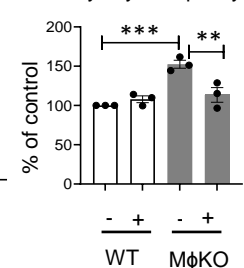
Glycolysis (ECAR)



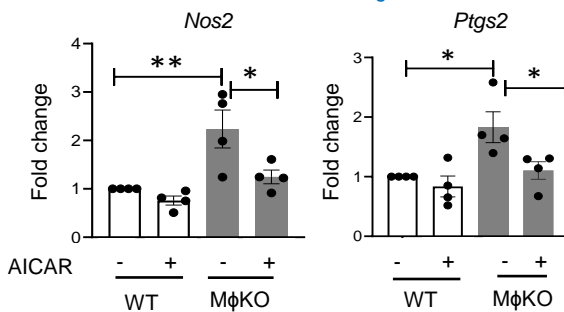
Glycolysis



Glycolytic capacity

**F**

M1-marker gene



M2-marker gene

